


Plasmonic-enhanced targeted nanohealing of metallic nanostructures

Cite as: Appl. Phys. Lett. **112**, 071108 (2018); <https://doi.org/10.1063/1.5018120>

Submitted: 04 December 2017 . Accepted: 06 February 2018 . Published Online: 16 February 2018

Hangbo Yang,  Jinsheng Lu, Pintu Ghosh, Ziyao Chen, Wei Wang, Hui Ye, Qian Yu, Min Qiu, and  Qiang Li



View Online



Export Citation



CrossMark

ARTICLES YOU MAY BE INTERESTED IN

[Optically controllable nanobreaking of metallic nanowires](#)

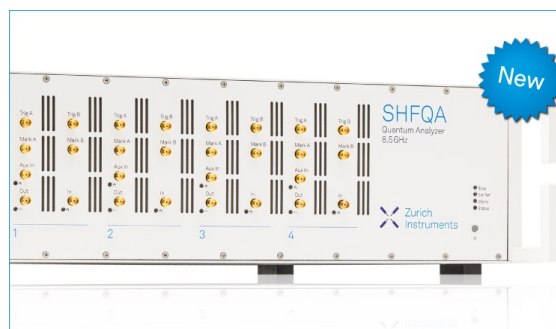
Applied Physics Letters **110**, 081101 (2017); <https://doi.org/10.1063/1.4976947>

[Near-field plasmonic beam engineering with complex amplitude modulation based on metasurface](#)

Applied Physics Letters **112**, 073104 (2018); <https://doi.org/10.1063/1.5013327>

[Plasmon-induced demagnetization and magnetic switching in nickel nanoparticle arrays](#)

Applied Physics Letters **112**, 072406 (2018); <https://doi.org/10.1063/1.5012857>



Your Qubits. Measured.

Meet the next generation of quantum analyzers

- Readout for up to 64 qubits
- Operation at up to 8.5 GHz, mixer-calibration-free
- Signal optimization with minimal latency

Find out more

 Zurich Instruments

Plasmonic-enhanced targeted nanohealing of metallic nanostructures

Hangbo Yang,¹ Jinsheng Lu,¹ Pintu Ghosh,¹ Ziyao Chen,¹ Wei Wang,¹ Hui Ye,¹ Qian Yu,² Min Qiu,¹ and Qiang Li^{1,a)}

¹State Key Laboratory of Modern Optical Instrumentation, College of Optical Science and Engineering, Zhejiang University, Hangzhou 310027, China

²Center of Electron Microscopy and State Key Laboratory of Silicon Materials, College of Materials Science and Engineering, Zhejiang University, Hangzhou 310027, China

(Received 4 December 2017; accepted 6 February 2018; published online 16 February 2018)

Healing defects of metallic structures is an essential procedure for manufacturing and maintaining integrated devices. Current nanocomposite-assisted microhealing methodologies are inadequate for nanoscopic applications because of their concomitant contamination and limited operation accuracy. In this paper, we propose an optically controllable targeted nanohealing technique by utilizing the plasmonic-enhanced photothermal effect. The healing of nanogaps between two silver nanowires (NWs) is achieved by increasing the incident laser power in steps. Partial connection of NWs can be readily obtained using this technique, while near-perfect connection of NWs with the same crystal orientations is obtained only when the lattices on the two opposing facets are matched after recrystallization. This non-contaminating nanohealing technique not only provides deeper insight into the heat/mass transfer assisted by plasmonic photothermal conversion in the nanoscale but also suggests avenues for recovering mechanical, electronic, and photonic properties of defected metallic nanodevices. *Published by AIP Publishing.* <https://doi.org/10.1063/1.5018120>

Healing is ubiquitous, from biological tissue to non-biological materials, from macroscope to nanoscope. In nature, the ability to heal injury increases the survivability and lifetime of most plants and animals. In artificial fields, healing materials after damage or fracture for prolonging their life-span and reducing their costs has a dramatic impact on micro/nano-scopic fields, including biomedicine,^{1–6} mechanics,^{7–12} photonics,^{13–23} and electronics.^{24–31}

Healing of microdefects (such as microcracks^{32–35} and microscratches^{15,36–38}) plays an important role in manufacture and maintenance of mechanic, electronic, and photonic micro-devices. Currently, most microhealing (induced by heat,^{38,39} moisture,^{32,33,40–42} and light^{15,36}) methodologies are implemented with the assistance of nanocomposites. In these microhealing processes, nanocomposites (such as metallic nanostructures¹⁵ and conductive polymers^{32,38,42}) are suspended and deposited to heal microdefects in order to restore the mechanical connection and electrical or optical conductivity of broken pathways. Although these methods can be utilized to heal many microdefects simultaneously, serious contamination of the adjacent intact parts might be caused by the non-targetedly dispersed nanocomposites, leading to crosstalk or short circuits. Besides, with mechanical, electronic, and photonic devices downsizing further to nanometer scale, these microhealing methods are inadequate for the nanoscopic applications due to the limitation of their operation accuracy.

Towards achieving fabrication and maintenance of nanodevices with minimized contamination, there has yet to emerge a viable solution to targetedly nanohealing the defects. In this regard, we present a plasmonic-enhanced targeted nanohealing technique with nanoscale accuracy. Nanogap, which is a kind of typical nanodefekt, is healed by

this technique. In the nanohealing process, continuous-wave (CW) laser shots with increasing power narrow the nanogap widths step by step. By appropriately controlling the exposure power, the partial connection (*i.e.*, the nanogap connected at its bottom) can be obtained. Furthermore, near-perfect connection (*i.e.*, connection of the nanowires (NWs) throughout the cross-section of the nanogap) of NWs with the same crystal orientation is obtained when the crystal orientations on the two opposing facets are matched. This nanohealing technique presents four advantageous traits: (i) superior targeting which minimizes the influence in the non-defect area, (ii) no extra contamination as the nanodefekt are healed by utilizing intrinsic materials, (iii) low cost since the CW laser is exploited in the nanohealing, and (iv) high flexibility and nanoscopic accuracy in operation rendered by the non-contact handling with CW laser and a microscope. Although Garnett's work has demonstrated the light-induced plasmonic welding technique,¹⁴ it works only for vertical nanogaps formed by two crossed nanowires. The technique presented in this work aims at healing parallel nanogaps, which is ubiquitous in defected nanocircuits, and its dynamic nanowelding process is also reported. This result unveils the role of plasmonic-enhanced photothermal conversion in heat/mass transfer at the nanometer scale, provides a distinct guideline on how to exploit this plasmonic effect for recovering properties of defected mechanical, photonic, and electronic nanodevices, and thereby can be potentially applied to photomask repair for integrated circuit fabrication and microchip package for nano-electromechanical systems.^{24–28}

Nanogaps in silver nanowires (NWs) as typical nanodefekt in metallic nanostructures are repaired by the plasmonic-enhanced targeted nanohealing technique presented in this article. The surface plasmon polaritons are excited when the nanogap is exposed to a focused CW laser, and thereafter, the optical energy is converted into thermal

^{a)}Email: qiangli@zju.edu.cn

energy owing to the decay of polaritons.^{43–49} As a result, the generated thermal energy elevates local temperature in and around the nanogap, causing atoms on the edges to move towards the nanogap center due to Rayleigh instability.⁷ After the laser exposure, the local temperature in and around the nanogap decreases, during which the resolidification of local movable silver atoms narrows the nanogap and connection of NWs is achieved.

Figure 1 shows the process of plasmonic-enhanced targeted nanohealing for nanogaps (initial gap width $g = 80$ nm, fabricated by cutting the NWs using focused ion beam, see Methods, [supplementary material](#)) between two silver NWs. The corresponding experimental apparatus is shown in [supplementary material](#) Fig. S1. The silver NWs with nanogaps are laid between two adjacent gold electrodes, which are used to monitor the recovery of the electric conductivity of nanowires by measuring the voltage-current (V-I) curve with a two-probe system (see [supplementary material](#) Methods). The silver NWs show typical pentagonal cross-sections [Fig. 1(c)]. The diameters (D) of silver NWs range from 200 nm to 400 nm, and their lengths are longer than 40 μm . Focused CW laser shots (wavelength $\lambda = 532$ nm, beam radius $R_b = 200$ nm, and exposure time $t = 2$ ms controlled by a mechanical shutter) are utilized to heal the nanogaps. The relationship between the absorptance of the silver NW ($D = 300$ nm for the nanowire and $g = 80$ nm for the nanogap) and the laser wavelength is calculated (shown in Fig. S4 in the [supplementary material](#)). For example, an 80-nm-wide nanogap between two silver NWs of diameter $D = 300$ nm is shown in Fig. 1(c-i). The nanohealing is achieved by increasing the incident laser power in steps. At first, the nanogap is exposed to laser shots with comparatively low constant power ($P = 30$ mW) with perpendicular polarization. The direction of the perpendicular polarization and parallel polarization is perpendicular and parallel to the axis of the NW, respectively. The perpendicular polarization is chosen because the maximum temperature of the nanogap under perpendicular polarization is less sensitive to nanogap widths compared with that under parallel polarization (Fig. S3 in the [supplementary material](#)). Low power is used at first because the initial nanogap ($g = 80$ nm) is prone to be damaged at high power. The gap width is reduced from 80 nm to 42 nm with several laser shots ($P = 30$ mW). Eventually, the

nanogap stops narrowing even with additional laser shots. In this process, the morphology of the edges of the pentagonal NWs at the nanogap end changes and becomes round shaped [Figs. 1(b-ii) and 1(c-ii)]. In the next step, the power of the laser shot is gradually increased from 30 mW to 60 mW with a step of 5 mW, and partial connection with the nanogap connected at its bottom is obtained at power $P = 60$ mW [Figs. 1(b-iii) and 1(c-iii)]. The bright field transmission electron microscopy (BFTEM) image of the cross-section of the connected part [from the slice marked with the red arrow in Fig. 1(c-iii)] illustrates its partial connection [Fig. 1(d)].

The V-I curves also demonstrate the recovery capability of electrical properties of the NW with a nanogap after nanohealing [Fig. 1(e)]. Before cutting the NW, the resistance of the NW (without a nanogap) comes out to be about 15 Ω (the blue line). After cutting (before nanohealing), the NW is disconnected and its resistance becomes infinite (the black line). After nanohealing, its resistance turns out to be about 18 Ω (the red line), showing that the nanohealing restores its original electrical conductivity although only partial connection of the two NWs is realized. The resistance of the connected part at the bottom of the nanogap can be estimated as 0.2 Ω according to the resistance equation $R = \rho l / (\pi r^2)$, where ρ ($= 1.65 \times 10^{-8}$ $\Omega\cdot\text{m}$ for bulk silver) is the resistivity of silver, l ($= 30$ nm) is the length of the connected part, and r ($= 10$ nm) is the radius of the connected part. Therefore, the resistance of the partial connection of the two NWs occupies only a small portion of the total resistance, and partial connection is enough to recover the original electrical conductivity.

The nanohealing with partial connection is achieved by increasing the incident laser power in steps and adjusting the number of laser shots. First, we mainly study the effects of laser power and NW diameter on narrowing the nanogap width for the first laser shot. Since nanohealing with partial connection cannot be obtained by the first laser shot, multiple laser shots continue to be imposed.

To study the effect of incident laser power on narrowing the nanogap width, different powers (20 mW–65 mW) are exploited to expose the nanogaps ($g = 100$ nm) in NWs with a similar diameter ($D \approx 340$ nm). Figure 2(a) shows the change of the nanogap width with increasing incident laser power. The nanogap width does not change when it is exposed to a laser shot of power $P \leq 25$ mW. Only when the

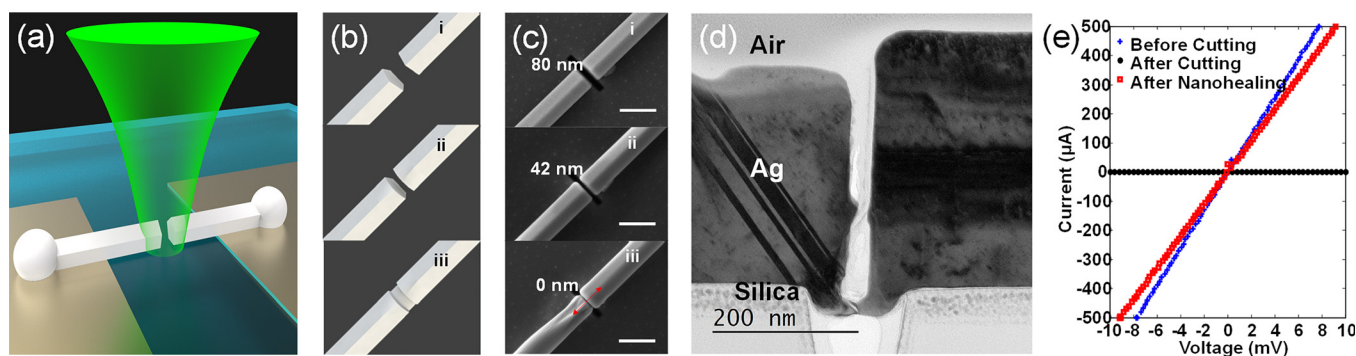


FIG. 1. Process of plasmonic-enhanced targeted nanohealing. (a) Schematic diagram depicting the healing technique of the nanogap between two silver NWs with laser shots. (b) Model diagrams and (c) SEM images of nanogap evolution in the healing process: the nanogap (i) before laser shots, (ii) after the first laser shot, and (iii) after multiple laser shots with increasing power. Inset scale bars represent 500 nm. (d) The BFTEM image of the cross-section of the connected part from the slice marked with a red arrow in (c-iii). The nanogap is partially connected at its bottom. The scale bar represents 200 nm. (e) Electrical characterization (V-I curves) of a silver NW before cutting, after cutting (before nanohealing), and after nanohealing is presented as blue, black, and red lines, respectively.

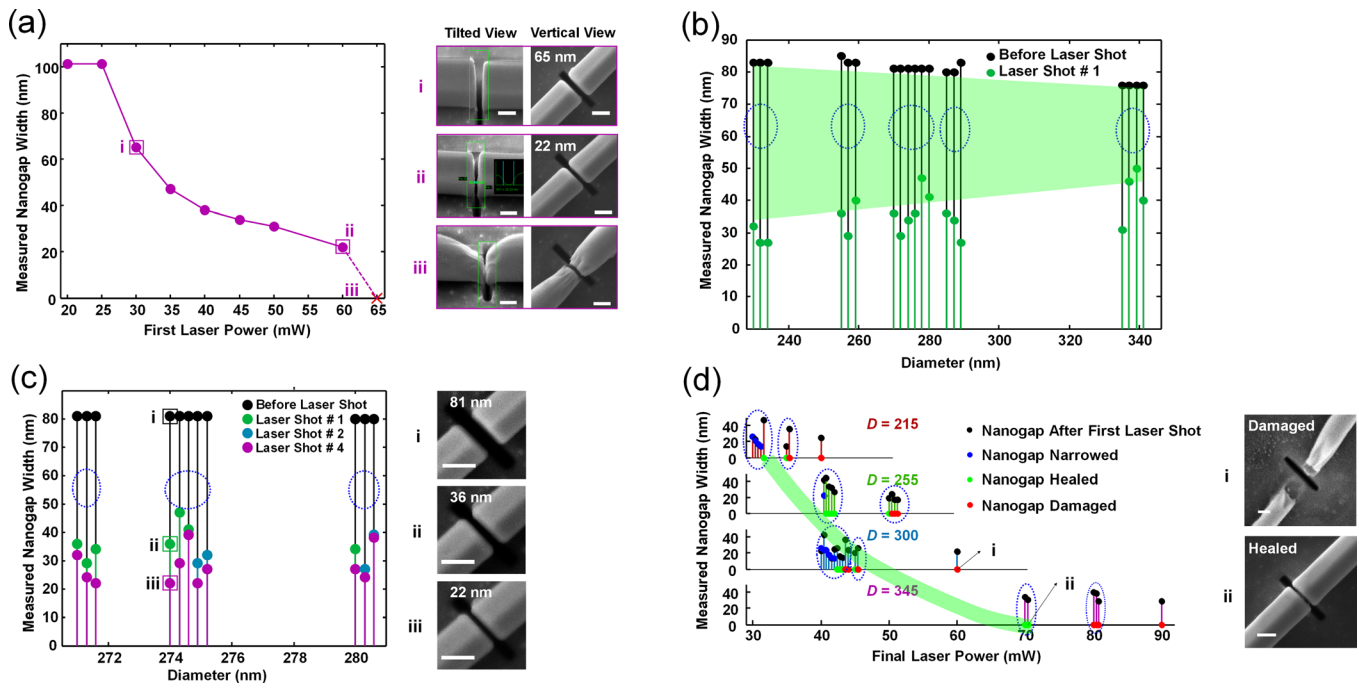


FIG. 2. The dependence of the change of the nanogap width on (a) and (d) laser power, (b) and (d) NW diameter, and (c) number of laser shots for (a) and (b) the first laser shot and (c) and (d) multiple laser shots. (a) Measured nanogap width versus laser power. Insets are SEM images of the nanogaps exposed to the laser shot with power $P = 30$ mW (c-i), 60 mW (c-ii), and 65 mW (c-iii). The insets in the tilted view are measured from the side view tilted at 54° . Inset scale bars represent 200 nm. (b) Measured nanogap width versus the NW diameter. Black and green dots represent nanogap widths before and after the laser shot, respectively. Vertical lines (marked with blue dashed circle) representing different nanogaps but corresponding to the same NW diameter are slightly shifted along the X-axis for the purpose of clarity. The semitransparent green trapezium represents the trend of the reduced amount of nanogap widths with increasing NW diameters. (c) For multiple laser shots with fixed laser power ($P = 30$ mW), measured nanogap widths with similar NW diameters ($D = 271$ nm, 274 nm, and 280 nm) versus number of laser shots ($N = 1, 2$, and 4). (d) For multiple laser shots with increasing laser power, measured nanogap widths versus final laser power (FLP). FLP here means the power of the ending laser shot exposed on the nanogap. The semitransparent green thick curve represents the trend of the required FLP for healing the NW with increasing NW diameters. Lines in the same blue dashed circle represent nanogaps exposed with the same power. Typical SEM images of the damaged and partially connected nanogaps (corresponding to the NW with diameter $D = 300$ nm) exposed to laser shots with FLP $P = (i) 40$ mW and $(ii) 60$ mW, respectively. Inset scale bars represent 200 nm.

power is beyond 30 mW does the nanogap width decrease [Fig. 2(a-i)]. The nanogap width becomes smaller as the incident laser power is increased. The nanogap width is reduced from the initial value 100 nm to 20 nm for the incident laser power $P = 60$ mW [Fig. 2(a-ii)]. The NWs get damaged when the incident power is increased beyond 60 mW [Fig. 2(a-iii)]. Since the initial nanogaps ($g = 100$ nm) are easy to be damaged by the high laser power, low initial laser power ($P = 30$ mW) is utilized in later nanohealing.

The effect of the NW diameter on narrowing the nanogap width is also investigated. Figure 2(b) shows the change of measured nanogap widths for different NW diameters (230 nm–340 nm) and the same initial nanogap width (around 80 nm) after the first laser shot ($N = 1$) of power $P = 30$ mW. The nanogap widths after one laser shot are reduced, compared with those before the laser shot (indicated by the black dots). The reduced amount of nanogap widths generally decreases as the NW diameter increases. For example, the nanogap widths for NWs of $D = 230$ nm are reduced by 55 nm, whereas the nanogap widths for NWs of $D = 340$ nm are reduced by 35 nm. This trend is in accord with the simulated results showing that the maximum temperatures of the nanogaps ($g = 80$ nm) decrease from 940 K to 680 K as the diameters of the NWs increase from 220 nm to 340 nm [Fig. S2(g) in the [supplementary material](#)]. The exact temperature for melting the NW cannot be identified in experiment. The calculated temperature in the gap is around 740 K for the

nanogap ($D = 300$ nm and $g = 80$ nm). The reduction of the nanogap width is due to the resolidification of movable surface atoms which flow towards the center of the nanogap. Therefore, it can be concluded that the nanogap width reduction is less for larger NW diameters as the maximum temperature decreases with increasing NW diameters.⁵⁰

The influence of multiple laser shots with fixed power on narrowing the nanogap width is investigated. Figure 2(c) shows the change of nanogap widths after different numbers of laser shots. The NWs corresponding to these nanogaps have similar diameters (271 nm, 274 nm, and 280 nm), and the initial nanogap widths are about 80 nm. The incident laser power is fixed at $P = 30$ mW. The nanogap width decreases to 36 nm and 22 nm after one laser shot and after four laser shots [Fig. 2(c)], respectively. The nanogap cannot be reduced below 20 nm even if the number of laser shots is increased further. This self-limited saturation in the amount of reduced nanogap widths results from the decreasing nanogap width at the nanogap because the maximum temperature declines with the decreasing nanogap width [Fig. S2(g), [supplementary material](#)].

Since nanohealing of the nanogaps cannot be achieved by increasing the number of laser shots with the same power, we continue to implement multiple laser shots with gradually raised laser power after the first laser shot of $P = 30$ mW. The laser power is not directly raised to high power, because the nanogaps with width $g = 40$ nm \pm 10 nm are easy to be

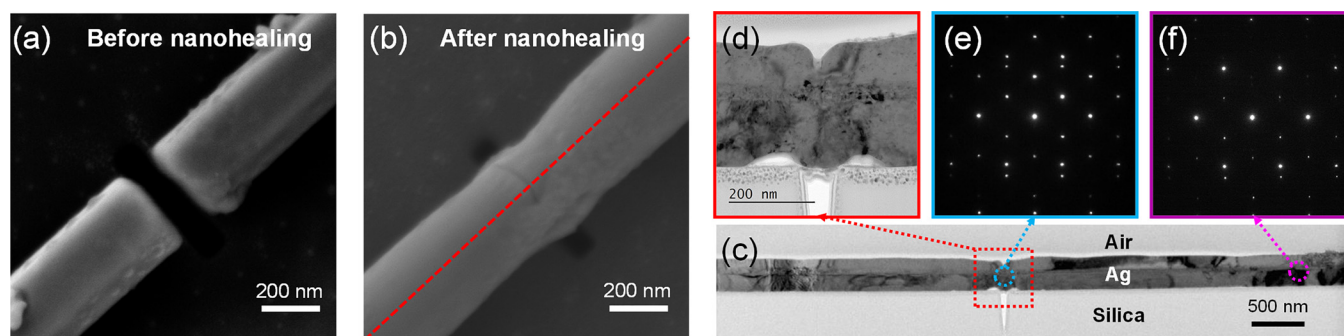


FIG. 3. Nanohealing with near-perfect connection. The nanogap (a) before and (b) after laser shots. (c) The BFTEM image of the cross-section of the connected part [marked as a red dashed line in (b)]. (d) The zoom-in image for a red rectangle in (c). (e) and (f) The SAED patterns for a blue circle and a pink circle in (c) show the silver lattice in (e) the connected part and (f) the original part, respectively.

damaged by the high laser power. Figure 2(d) shows the dependence of the change of nanogap widths on the NW diameters and incident laser power. Nanohealing with partial connection for nanogaps corresponding to NWs with four different diameters ($D = 215$ nm, 255 nm, 300 nm, and 345 nm) is obtained in this study. The power of the laser shots is increased from 30 mW to 60 mW with a step of 5 mW and further from 60 mW to 90 mW with a step of 10 mW. The nanogaps corresponding to the NWs with the same diameter are narrowed, healed (with partial connection), and damaged (cannot be healed with this technique any more) sequentially with increasing incident laser power. Thus, healing nanogaps requires appropriate final laser power (FLP). For instance, the nanogaps corresponding to the NWs with diameter $D = 215$ nm are narrowed at power $P = 30$ mW, nanohealed at power $P = 35$ mW, and damaged at power $P = 35$ or 40 mW. For the NWs with larger diameters, the required final laser power for healing is higher. According to the simulated maximum temperature corresponding to incident power $P = 40$ mW for different NW diameters (220 nm–340 nm) in Fig. S2(g) (supplementary material), to achieve the same maximum temperature, the nanogaps corresponding to NWs with larger diameters require higher final laser power. These simulated results agree with the experimental results shown in Fig. 2(d).

Besides nanohealing with partial connection, we also obtain nanohealing with near-perfect connection of NWs (Fig. 3). The nanogap ($g = 80$ nm) corresponding to the NW of diameter $D = 320$ nm [Fig. 3(a)] is healed with near-perfect connection after five laser shots ($P = 30$ mW, 40 mW, 50 mW, 60 mW, and 60 mW; $t = 2$ ms, 2 ms, 2 ms, 2 ms, and 125 ms). About 70% of the gap area is healed. This near-perfect connection was achieved as the two sides had the same crystal orientation after laser-induced recrystallization. Figures 3(c) and 3(d) show the cross-sectional BFTEM images of the healed nanowire; the sample was lift-out from the red dashed line in Fig. 3(b) by using the focused ion beam. It is clear that the crystal orientation of the healed part [blue circle in Fig. 3(c)] is consistent with that of the original part [purple circle in Fig. 3(c)], since the selected area electron diffraction (SAED) patterns [Figs. 3(e) and 3(f)] from the two parts show the consistency.

In conclusion, we have proposed a technique of plasmonic-enhanced targeted nanohealing. Nanogap as a kind of typical nanodefekt is healed by this technique. The

nanohealing is achieved by increasing the incident laser power in steps and adjusting the number of laser shots. Laser shots with increasing power at the nanogap step by step cause the local temperature to rise and more local silver atoms of the NWs to move towards the nanogap. By appropriately controlling the exposure power, nanohealing with partial connection can be obtained. Furthermore, we obtain a near-perfect connection of NWs with the same crystal orientation. This technique reveals the role of the photothermal conversion in heat/mass transfer in the nanoscale and offers a platform to exploit the enhanced properties of mechanical, photonic, and electronic nanodevices.

See [supplementary material](#) for (1) experimental apparatus, (2) simulation results corresponding to nanohealing, (3) simulations for polarization analysis, (4) simulation of the dependence of absorptance on wavelength, and (5) methods.

This work was supported by the National Key Research and Development Program of China (No. 2017YFA0205700) and the National Natural Science Foundation of China (Grant Nos. 61775194, 61425023, and 61575177).

- ¹A. Goel and V. Vogel, *Nat. Nanotechnol.* **3**, 465 (2008).
- ²F. Olasagasti, K. R. Lieberman, S. Benner, G. M. Cherf, J. M. Dahl, D. W. Deamer, and M. Akeson, *Nat. Nanotechnol.* **5**, 798 (2010).
- ³A. M. Khawaja, *Int. J. Surg.* **9**, 608 (2011).
- ⁴W. Gao and J. Wang, *Nanoscale* **6**, 10486 (2014).
- ⁵S. J. Heerema and C. Dekker, *Nat. Nanotechnol.* **11**, 127 (2016).
- ⁶C. L. Smith, A. H. Thilsted, J. N. Pedersen, T. H. Youngman, J. C. Dyrnum, N. A. Michaelsen, R. Marie, and A. Kristensen, *ACS Nano* **11**, 4553 (2017).
- ⁷P. Peng, Z. Su, Z. Liu, Q. Yu, Z. Cheng, and J. Bao, *Nanoscale* **5**, 9532 (2013).
- ⁸K. K. Kim, S. Hong, H. M. Cho, J. Lee, Y. D. Suh, J. Ham, and S. H. Ko, *Nano Lett.* **15**, 5240 (2015).
- ⁹Q. Nian, M. Saei, Y. Xu, G. Sabyasachi, B. Deng, Y. P. Chen, and G. J. Cheng, *ACS Nano* **9**, 10018 (2015).
- ¹⁰K. Cai, J. Yu, J. Wan, H. Yin, J. Shi, and Q. H. Qin, *Carbon* **101**, 168 (2016).
- ¹¹K. Kim, J. Guo, Z. Liang, F. Zhu, and D. Fan, *Nanoscale* **8**, 10471 (2016).
- ¹²C. Shi, D. K. Luu, Q. Yang, J. Liu, J. Chen, C. Ru, S. Xie, J. Luo, J. Ge, and Y. Sun, *Microsyst. Nanoeng.* **2**, 16024 (2016).
- ¹³X. Wang and Y. Lu, *J. Appl. Phys.* **98**, 114304 (2005).
- ¹⁴E. C. Garnett, W. Cai, J. J. Cha, F. Mahmood, S. T. Connor, M. G. Christoforo, Y. Cui, M. D. McGehee, and M. L. Brongersma, *Nat. Mater.* **11**, 241 (2012).
- ¹⁵A. U. Zillohu, R. Abdelaziz, M. K. Hedayati, T. Emmmler, S. Homaeigohar, and M. Elbahri, *J. Phys. Chem. C* **116**, 17204 (2012).

- ¹⁶S. Han, S. Hong, J. Ham, J. Yeo, J. Lee, B. Kang, P. Lee, J. Kwon, S. S. Lee, and M. Y. Yang, *Adv. Mater.* **26**, 5808 (2014).
- ¹⁷S. R. Das, Q. Nian, M. Saei, S. Jin, D. Back, P. Kumar, D. B. Janes, M. A. Alam, and G. J. Cheng, *ACS Nano* **9**, 11121 (2015).
- ¹⁸G. González-Rubio, J. S. González-Izquierdo, L. Bañares, G. Tardajos, A. Rivera, T. Altantzis, S. Bals, O. Peña-Rodríguez, A. Guerrero-Martínez, and L. M. Liz-Marzán, *Nano Lett.* **15**, 8282 (2015).
- ¹⁹H. Yang, M. Qiu, and Q. Li, *Laser Photonics Rev.* **10**, 278 (2015).
- ²⁰S. Dai, Q. Li, G. Liu, H. Yang, Y. Yang, D. Zhao, W. Wang, and M. Qiu, *Appl. Phys. Lett.* **108**, 121103 (2016).
- ²¹Q. Li, G. Liu, H. Yang, W. Wang, S. Luo, S. Dai, and M. Qiu, *Appl. Phys. Lett.* **108**, 193101 (2016).
- ²²L. Zhou, J. Lu, H. Yang, S. Luo, W. Wang, J. Lv, M. Qiu, and Q. Li, *Appl. Phys. Lett.* **110**, 081101 (2017).
- ²³J. H. Park, G. T. Hwang, S. Kim, J. Seo, H. J. Park, K. Yu, T. S. Kim, and K. J. Lee, *Adv. Mater.* **29**, 9 (2016).
- ²⁴P. Heard, J. Cleaver, and H. Ahmed, *J. Vac. Sci. Technol. B* **3**, 87 (1985).
- ²⁵A. Wagner, J. Levin, J. Mauer, P. Blauner, S. Kirch, and P. Longo, *J. Vac. Sci. Technol. B* **8**, 1557 (1990).
- ²⁶T. Liang, A. Stivers, R. Livengood, P.-Y. Yan, G. Zhang, and F.-C. Lo, *J. Vac. Sci. Technol. B* **18**, 3216 (2000).
- ²⁷A. Yasaka, F. Aramaki, M. Muramatsu, T. Kozakai, O. Matsuda, Y. Sugiyama, T. Doi, O. Takaoka, R. Hagiwara, and K. Nakamae, *J. Vac. Sci. Technol. B* **26**, 2127 (2008).
- ²⁸J. H. Noh, M. Stanford, B. Lewis, J. D. Fowlkes, H. Plank, and P. Rack, *Appl. Phys. A* **117**, 1705 (2014).
- ²⁹T. A. Celano, D. J. Hill, X. Zhang, C. W. Pinion, J. D. Christesen, C. J. Flynn, J. R. McBride, and J. F. Cahoon, *Nano Lett.* **16**, 5241 (2016).
- ³⁰L. Lin, L. Liu, K. Musselman, G. Zou, W. W. Duley, and Y. N. Zhou, *Adv. Funct. Mater.* **26**, 5979 (2016).
- ³¹Y. Yao, K. K. Fu, S. Zhu, J. Dai, Y. Wang, G. Pastel, Y. Chen, T. Li, C. Wang, and T. Li, *Nano Lett.* **16**, 7282 (2016).
- ³²S. R. White, N. Sottos, P. Geubelle, J. Moore, M. R. Kessler, S. Sriram, E. Brown, and S. Viswanathan, *Nature* **409**, 794 (2001).
- ³³Y. Chen, A. M. Kushner, G. A. Williams, and Z. Guan, *Nat. Chem.* **4**, 467 (2012).
- ³⁴S. A. Odom, S. Chayanupatkul, B. J. Blaiszik, O. Zhao, A. C. Jackson, P. V. Braun, N. R. Sottos, S. R. White, and J. S. Moore, *Adv. Mater.* **24**, 2578 (2012).
- ³⁵M. Amjadi, M. Turan, C. P. Clementson, and M. Sitti, *ACS Appl. Mater. Interfaces* **8**, 5618 (2016).
- ³⁶B. Ghosh and M. W. Urban, *Science* **323**, 1458 (2009).
- ³⁷Y. Li, S. Chen, M. Wu, and J. Sun, *Adv. Mater.* **24**, 4578 (2012).
- ³⁸B. C. Tee, C. Wang, R. Allen, and Z. Bao, *Nat. Nanotechnol.* **7**, 825 (2012).
- ³⁹X. Chen, M. A. Dam, K. Ono, A. Mal, H. Shen, S. R. Nutt, K. Sheran, and F. Wudl, *Science* **295**, 1698 (2002).
- ⁴⁰P. Cordier, F. Tournilhac, C. Soulié-Ziakovic, and L. Leibler, *Nature* **451**, 977 (2008).
- ⁴¹Q. Wang, J. L. Mynar, M. Yoshida, E. Lee, M. Lee, K. Okuro, K. Kinbara, and T. Aida, *Nature* **463**, 339 (2010).
- ⁴²C. Wang, N. Liu, R. Allen, J. B. H. Tok, Y. Wu, F. Zhang, Y. Chen, and Z. Bao, *Adv. Mater.* **25**, 5785 (2013).
- ⁴³X. Chen, Y. Chen, M. Yan, and M. Qiu, *ACS Nano* **6**, 2550 (2012).
- ⁴⁴G. Baffou and R. Quidant, *Laser Photonics Rev.* **7**, 171 (2013).
- ⁴⁵T.-B. Song, Y. Chen, C.-H. Chung, Y. Yang, B. Bob, H.-S. Duan, G. Li, K.-N. Tu, Y. Huang, and Y. Yang, *ACS Nano* **8**, 2804 (2014).
- ⁴⁶A. T. Bellew, H. G. Manning, C. Gomes da Rocha, M. S. Ferreira, and J. J. Boland, *ACS Nano* **9**, 11422 (2015).
- ⁴⁷Y.-J. Shiao, K.-M. Chiang, and H.-W. Lin, *Nanoscale* **7**, 12698 (2015).
- ⁴⁸J. A. Spechler, K. A. Nagamatsu, J. C. Sturm, and C. B. Arnold, *ACS Appl. Mater. Interfaces* **7**, 10556 (2015).
- ⁴⁹L. Lin, G. Zou, L. Liu, W. W. Duley, and Y. N. Zhou, *Appl. Phys. Lett.* **108**, 203107 (2016).
- ⁵⁰H.-L. Chen, S.-P. Ju, S.-L. Wang, C.-T. Pan, and C.-W. Huang, *J. Phys. Chem. C* **120**, 12840 (2016).